



# Effect of barium doping on the physical properties of zinc oxide nanoparticles elaborated via sonochemical synthesis method

KEKELI N'KONOU<sup>1,2</sup>, MUTHIAH HARIS<sup>2,\*</sup>, YENDOUBÉ LARE<sup>1</sup>,  
MAZABALO BANETO<sup>1</sup> and KOSSI NAPO<sup>1</sup>

<sup>1</sup>Laboratoire sur l'Énergie Solaire, Université de Lomé, BP 1515, Lomé – Togo

<sup>2</sup>Department of Physics, Karunya University, Coimbatore 641 114, India

\*Corresponding author. E-mail: harismuthiah@gmail.com

MS received 10 February 2015; revised 20 July 2015; accepted 7 September 2015; published online 9 June 2016

**Abstract.** The aim of this work is to study the effect of barium (Ba) doping on the optical, morphological and structural properties of ZnO nanoparticles. Undoped and Ba-doped ZnO have been successfully synthesized via sonochemical method using zinc nitrate, hexamethylenetetramine (HMT) and barium chloride as starting materials. The structural characterization by XRD and FTIR shows that ZnO nanoparticles are polycrystalline with a standard hexagonal ZnO wurtzite crystal structure. Decrease in lattice parameters from diffraction data shows the presence of Ba<sup>2+</sup> in the ZnO crystal lattice. The morphology of the ZnO nanoparticles has been determined by scanning electron microscopy (SEM). Incorporation of Ba was confirmed from the elemental analysis using EDX. Optical analysis depicted that all samples exhibit an average optical transparency over 80%, in the visible range. Room-temperature photoluminescence (PL) spectra detected a strong ultraviolet emission at 330 nm and two weak emission bands were observed near 417 and 560 nm. Raman spectroscopy analysis of Ba-doped samples reveals the successful doping of Ba ions in the host ZnO.

**Keywords.** Ba-doped ZnO; nanoparticles; sonochemical synthesis; Fourier transform infrared; Raman.

**PACS Nos** 81.05.Dz; 81.07.Bc; 81.07.Wx

## 1. Introduction

Zinc oxide (ZnO) has drawn the attention of many research groups over the last few years because this wide direct band gap (~3.37 eV) semiconductor shows promising application in nanoelectronics and optoelectronics industry [1]. Most of the research in sonochemically synthesized zinc oxide (ZnO) nanoparticles (NPs) has led to significant theoretical and technological progresses since 2004 [2]. Chemical reactions involving zinc compounds in aqueous solutions are able to produce ZnO powders [3]. Under ultrasonic irradiation, sonochemical reactions result in ZnO with morphologies different from that synthesized by conventional methods. Different techniques have been developed to synthesize ZnO NPs, such as hydrothermal [4], chemical vapour deposition (CVD) [5], polymerization method [6], precipitation [7] oxidation process [8], ultrasonic assisted [9–15], sol–gel combustion [16] and mechanochemical processing [17]. The sonochemical

synthesis of the nanomaterial has been confirmed to be a simple and feasible technique to produce novel materials with different properties, because this method can generate similar truncated nanorods with small size as compared to other techniques [18–20]. This technique is a simple, green, rapid and feasible technique, as it does not require high temperature and/or highly toxic chemicals. The study of chemical effects of ultrasound arises from acoustic cavitation such as the development, growth and implosive collapse of bubble in liquid. The implosive collapse of bubble generates localized hot spots through shock wave formation within the gas phase of the collapsing bubble or adiabatic compression [21]. Interestingly, in the literature, zinc nitrate (Zn(NO<sub>3</sub>)<sub>2</sub>·6H<sub>2</sub>O) and hexamethylenetetramine (HMT) were used as starting materials to synthesize ZnO nanoparticles using sonochemical method [22,23].

It is well-known that ZnO nanoparticles doped with various transition metals are promising candidates

for a variety of practical applications. Among these metal dopants, Ba doping seems to be a promising one due to its applications in varistors [24] and liquid sensors' guiding layers [25]. There are very few reports available in literature on Ba-doped ZnO nanomaterials. Low-cost thermal decomposition method was used to investigate the influence of Ba doping on the ferroelectric and physical properties of ZnO nanoparticles [26]. Synthesis of Ba-doped ZnO nanoparticles by homogeneous precipitation method under ambient conditions and evaluation of their catalytic activity have been reported by Rajabi *et al* [27]. In the available literature, there is no report on sonochemical synthesis of Ba-doped ZnO nanoparticles. The objective of this present work is to prepare undoped and Ba-doped ZnO nanoparticles and investigate the influence of barium (Ba) doping concentrations on the structural, morphological and optical properties of ZnO nanoparticles using sonochemical synthesis method. The results of this investigation contribute to the application of synthesized nanostructures in optoelectronics devices.

## 2. Experimental procedure

### 2.1 Materials

Reagent-grade zinc nitrate ( $\text{Zn}(\text{NO}_3)_2 \cdot 6\text{H}_2\text{O}$ ), barium chloride ( $\text{BaCl}_2 \cdot 2\text{H}_2\text{O}$ ) and hexamethylenetetramine (HMT) powders (99.0% pure) were used as precursors without any pretreatment.

### 2.2 Synthesis

ZnO nanoparticles were synthesized by the sonochemical reaction between 0.05  $\text{Zn}(\text{NO}_3)_2$  and 0.05 M HMT. The solution was prepared by dissolving 2.97 g of  $\text{Zn}(\text{NO}_3)_2$  in 100 ml deionized water and stirring at 300 rpm for 10 min. After adding 1.4 g of HMT under continuous stirring, specific amount of barium chloride ( $\text{BaCl}_2 \cdot 2\text{H}_2\text{O}$ ) was introduced sequentially. ZnO nanoparticles doped with 1 at% and 2 at% of barium are denoted as  $\text{Ba}_1\text{ZnO}$  and  $\text{Ba}_2\text{ZnO}$ , respectively. The reaction solution was heated and kept at  $50^\circ\text{C}$  for 10 min. Once the solution is changed into a steady viscous white colloid, the stirring was continued for another 10 min. The colloid was then transferred to an ultrasonic bath (CupHorn Sonicator, Model-Heilscher UP 400s) which, at the maximum electrical power of 400 W, supplied a continuous 24 kHz ultrasonic wave under ambient conditions for 20 min. The white precipitate was recuperated by filtration and rinsed four times with ethanol and distilled water, after sonication.

The precipitate obtained was dried in an oven at  $100^\circ\text{C}$  in air for 6 h. The final products were collected for further characterizations.

### 2.3 Characterization

The crystalline phase of pure and barium-doped ZnO nanoparticles were analysed by X-ray diffractometry and the crystallite size ( $D$ ) was calculated from Scherrer's equation  $D = k\lambda/\beta \cos\theta$ , where  $\beta$  is the full-width at half-maximum (FWHM) of the peak,  $\theta$  is the diffraction angle,  $\lambda$  is the wavelength of the X-ray beam ( $\text{CuK}_\alpha \approx 1.5406 \text{ \AA}$ ) and  $k$  is the shape factor equal to 0.9. Scanning electron microscope (SEM) close-fitting with an energy dispersive X-ray spectroscopy (EDX) (JEOL JSM-840A) were used for elemental analysis and for analysing the surface morphology of the prepared nanoparticles. Transmittance and optical absorbance of the undoped and Ba-doped ZnO NPs were measured using UV-Vis spectrophotometer (JASCO, V-630) at room temperature. Spectrofluorescence (JASCO, FP-8200) with an excitation source of wavelength 325 nm was used to study the luminescence property of the synthesized nanoparticles at room temperature. The Fourier transform infrared (FTIR) measurements were recorded between 400 and  $4000 \text{ cm}^{-1}$  wavenumbers with a (Shimadzu) Fourier transform spectrometer. Raman spectra were recorded in the range of  $100\text{--}700 \text{ cm}^{-1}$  by a spectrophotometer (HORIBA JOBIN YVON T64000 operated using 30 mW He-Ne red laser with 632 nm wavelength).

## 3. Results and discussion

### 3.1 Structural characterization

The X-ray diffraction (XRD) spectra of the undoped and barium-doped ZnO nanoparticles are shown in figure 1a. All samples exhibit sharp diffraction peaks conforming to (2 0 0), (1 0 3), (1 1 0), (1 0 2), (1 0 1), (0 0 2) and (1 0 0) planes of wurtzite hexagonal ZnO structure in conformity with the database of the JCPDS number 36-1451. However, it is noticed that the diffraction peaks conforming to (1 0 2), (1 1 0), (1 0 3) and (2 0 0) planes appeared when the dopant amount was increased to 1 at% and the intensity of these peaks significantly increased unlike 2 at% Ba-doped ZnO. No secondary phase was detected in the XRD patterns of the doped samples. It can be observed from figure 1 that the appearance of secondary phase beyond 1 at% of Ba doping level indicates the destruction of

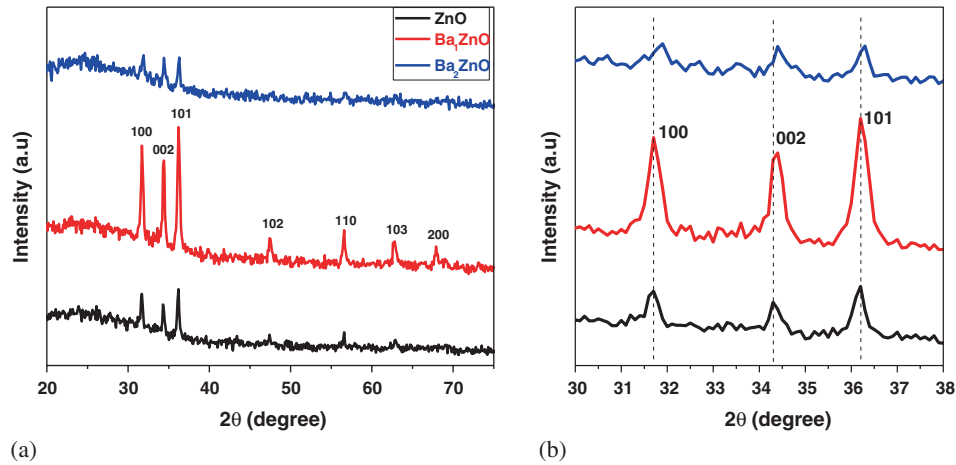


**Figure 1.** XRD patterns at (a)  $2\theta = 25^\circ\text{--}50^\circ$  and (b)  $2\theta = 33^\circ\text{--}37^\circ$  of Ba-doped and undoped ZnO NPs. Curve in black indicates undoped ZnO, red indicates  $\text{Ba}_1\text{ZnO}$  and blue indicates  $\text{Ba}_2\text{ZnO}$ .

the structure quality. The diffractograms exhibited that  $\text{Ba}^{2+}$  ions of the doped ZnO samples were only incorporated in the ZnO lattice. Figure 1b shows the change in the  $2\theta$  angle of the diffraction planes of (1 0 0), (0 0 2) and (1 0 1) peaks at  $2\theta = 30^\circ\text{--}38^\circ$  for undoped and Ba-doped ZnO NPs. The diffraction peaks translocated to higher  $2\theta$  due to the large radius of the Ba atom. To identify the effect of Ba doping on the samples, the lattice parameters  $a$  and  $c$  are calculated by using eq. (1), where  $d_{hkl}$  is the crystalline surface distance for  $hkl$  indices.

$$\frac{1}{d_{hkl}^2} = \frac{4}{3a^2}(h^2 + hk + k^2) + \frac{l^2}{c^2}. \quad (1)$$

Similarly, eq. (2) is employed to calculate the unit cell volume

$$V = \frac{\sqrt{3}a^2c}{2}, \quad (2)$$

where  $a$  and  $c$  are lattice parameters. To calculate the crystallite size, the (1 0 1) plane (the strongest) was selected and the dislocation density  $\delta$  which represents

the amount of defects in the nanoparticles was determined using the formula (3):

$$\delta = \frac{1}{D^2}, \quad (3)$$

which are tabulated in table 1. As shown in table 1, decrease of crystallite size was observed for the doped samples which are attributed to the inclusion of dopant into the Zn sites. In addition, the ratio of lattice constants ( $c/a$ ) was approximately equal to 1.60, for all samples. This result is in good agreement with values of the bulk wurtzite ZnO.

### 3.2 SEM with EDX characterizations

The surface morphologies of the prepared samples were characterized by SEM, as depicted in figure 2. The SEM images obviously showed different morphologies of undoped and Ba-doped ZnO NPs and nanostructural homogeneities. The SEM result showed the presence of agglomerated nanospheres. To that purpose, rough morphology was found in figure 2. It is noticed that the crystal becomes compact by increasing the dopant level. However, the crystallite sizes of the nanoparticles decrease from 25 to 12 nm with the

**Table 1.** Structural parameters of Ba-doped and undoped ZnO nanoparticles.

Sample	$2\theta$ value along (1 0 1) plane	Crystallite size $D$ (nm)	Dislocation density $\delta \times 10^{14}$ (lines/m <sup>2</sup> )	Lattice parameters (Å)		$c/a$ ratio	Volume (Å <sup>3</sup> )
				$a$	$c$		
ZnO	36.1386	25.53	15.34	3.26	5.22	1.60	48.08
$\text{Ba}_1\text{ZnO}$	36.1938	23.37	18.31	3.25	5.21	1.60	47.93
$\text{Ba}_2\text{ZnO}$	36.2109	12.59	63.09	3.24	5.20	1.60	47.52

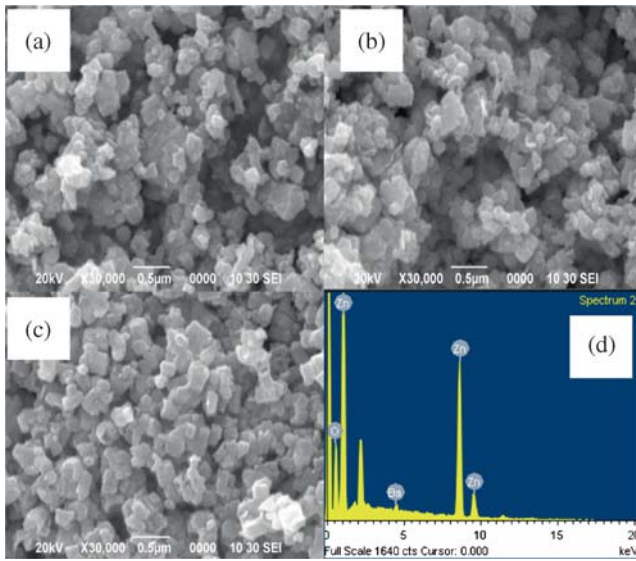


**Figure 2.** SEM micrographs of Ba-doped and undoped ZnO NPs. (a) ZnO; (b) Ba<sub>1</sub>ZnO; (c) Ba<sub>2</sub>ZnO and (d) EDX spectrum of Ba<sub>2</sub>ZnO sample.

increase in dopant level. It can be seen from the SEM images that particles size of ZnO varied in the range of 100–200 nm. It can be deduced that Ba doping slightly influenced the surface morphology and the grain size depending on the dopant level.

The elemental analysis of Ba-doped ZnO nanoparticles was carried out by energy dispersive X-ray (EDX) analysis. Figure 2d shows typical EDX spectrum of 2 at% Ba-doped ZnO nanoparticles. The presence of Ba, Zn and O without contamination by any other element was confirmed by EDX spectrum analysis. According to experiments, the expected Ba/Zn ratio is 0.02 in the samples. However, Ba/Zn ratio obtained in the Ba<sub>2</sub>ZnO sample is 0.0285. This indicates that the amount of Ba incorporation in the Ba<sub>2</sub>ZnO sample is slightly bigger than the amount of Ba in the starting solution. From this study, the presence of a small amount of barium particles in the system is identified which is also confirmed by the phase purity of XRD.

### 3.3 Photoluminescence spectroscopy

Figure 3 depicts the room-temperature photoluminescence (PL) spectra of Ba-doped ZnO and undoped ZnO under the excitation of 325 nm, which is an ordinary method for the investigation of intrinsic point defects in ZnO such as oxygen vacancies, interstitial zinc, interstitial oxygen and zinc vacancies. Vaguely, the PL of ZnO NPs shows one or more emission peaks in the visible spectral range and one emission peak in the UV region due to a recombination of free excitons,

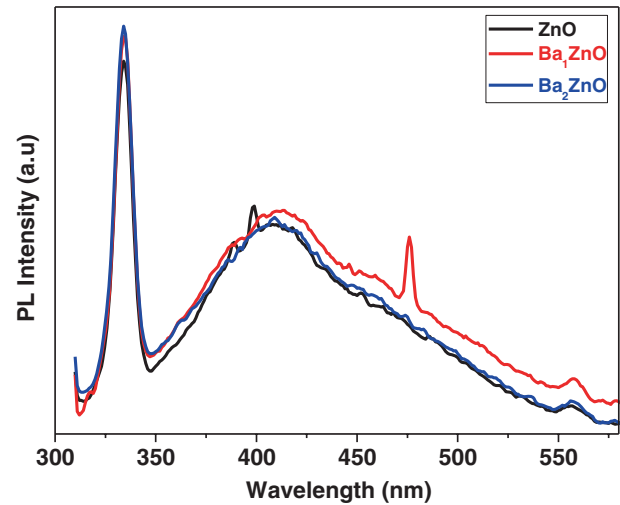


**Figure 3.** Photoluminescence spectra of Ba-doped and undoped ZnO.

which are assigned to defect emissions [24]. As shown in figure 3, undoped and Ba-doped ZnO samples exhibit sharp and strong ultraviolet (UV) emission peaks near 330 nm belonging to the exciton recombination equivalent to near band-edge (NBE) emission. Two emission bands observed near 417 and 560 nm are assigned to intrinsic defects such as the radiative recombination of delocalized electrons near the conduction band with profoundly trapped holes in oxygen centres and zinc interstitial, respectively [28,29]. The electron transition from the level of the ionized oxygen vacancies to the valence band can explain the emission observed around 475 nm as noticed in the case of 1 at% Ba-doped ZnO [30].

A nearly similar feature of the obtained PL spectra with slight enhancement in the intensity was observed for the undoped ZnO as compared to Ba-doped ZnO spectra. This slight enhancement for the PL spectra due to the incorporation of Ba dopant in the ZnO host material may be attributed to the increased number of defects in the material and surface states as discussed by Wang *et al* [31]. However, the strong visible emissions in doped ZnO NP samples may probably occur due to the electronic transitions from the deep levels, surface states levels to conduction band.

### 3.4 UV-Vis absorption characterization

Figure 4 shows the absorption of the corresponding UV-Vis spectra of the undoped and Ba-doped ZnO nanoparticles. The UV-Vis spectra showed that the lowest absorption is obtained with Ba<sub>2</sub>ZnO samples. The intensity of the absorption spectra in the higher energy region increases from the undoped ZnO to 1

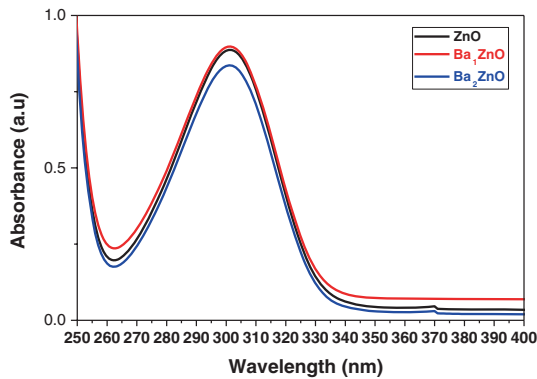


**Figure 4.** UV-Vis absorbance spectra of Ba-doped and undoped ZnO.

at% Ba-doped ZnO, after which the intensity decreases. This strong absorption means that the incoming photons have sufficient energy to stimulate electrons from the valence band to the conduction band.

Figure 5 shows the spectral behaviour of the normal incidence transmittance  $T(\lambda)$  for the Ba-doped ZnO and undoped ZnO NPs. As observed in figure 5, all samples exhibit an average optical transparency over 80%, in the visible range. It is obviously clear from the transmittance spectra that Ba<sub>2</sub>ZnO sample acquires better transparency compared to pure ZnO and Ba<sub>1</sub>ZnO samples, especially above 400 nm wavelength. Also, a little dependence is observed for the measured transmittance on the doping concentration of Ba at the studied range, especially near the band edge.

### 3.5 Fourier transform infrared (FTIR) analysis

Figure 6 shows the FTIR spectra of Ba-doped and undoped ZnO NPs. The FTIR spectra of the Ba-doped ZnO and undoped ZnO nanoparticles contain several bands without standing features. The spectral

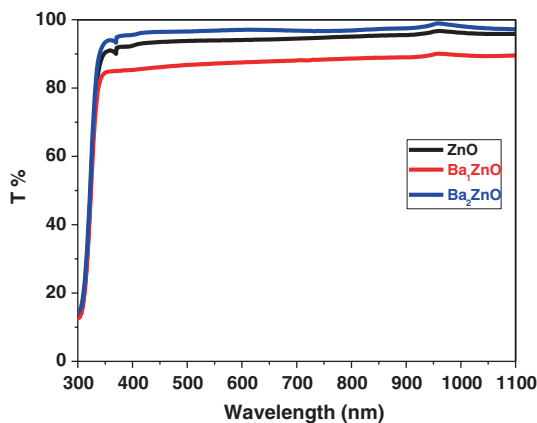


**Figure 5.** Transmission spectra of Ba-doped and undoped ZnO NPs.

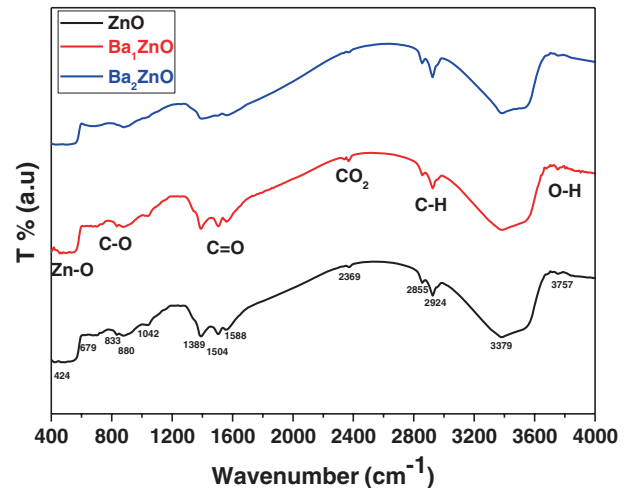


**Figure 6.** FTIR spectra of Ba-doped and undoped ZnO NPs.

bands observed at 424 and 679  $\text{cm}^{-1}$  for undoped ZnO, at 455, 495 and 679  $\text{cm}^{-1}$  for Ba<sub>1</sub>ZnO, at 440 and 494  $\text{cm}^{-1}$  for Ba<sub>2</sub>ZnO are correlated to metal oxide bond and distinctly show the presence of ZnO as reported in [32]. It is well-known that the peaks in the range of 400–700  $\text{cm}^{-1}$  correspond to ZnO stretching modes as reported by Saleh *et al* [33]. Bands at 880, 1042, 1389 and 1504  $\text{cm}^{-1}$  for undoped and Ba<sub>1</sub>ZnO and band at 1397  $\text{cm}^{-1}$  for Ba<sub>2</sub>ZnO are attributed to the bending frequency and oxygen stretching modes [34]. The presence of absorption peak around 2369  $\text{cm}^{-1}$  observed in the undoped and Ba<sub>1</sub>ZnO shows the existence of CO<sub>2</sub> molecules in air and those at 2800–3000  $\text{cm}^{-1}$  is due to C–H stretching frequencies. Bands are found to be blue shifted at 3379, 3757 and 3875  $\text{cm}^{-1}$  indicating the presence of OH group in undoped and Ba-doped ZnO respectively. The Zn–O–Zn network is disrupted by the existence of Ba in its environment. This disruption explains the shift in the peak position of the ZnO absorption bands observed by the XRD analysis.

### 3.6 Raman spectroscopy analysis

Raman spectroscopy was used to investigate dopant incorporation, crystal quality for various ZnO nanostructure induced defects, and disorder in the ZnO lattice or to mark the possible secondary oxide. Raman spectra of Ba-doped ZnO and undoped ZnO NPs from 100 to 700  $\text{cm}^{-1}$  are shown in figure 7. Depending on the group theory, two formula units per cell and eight sets of optical phonon modes at the  $\Gamma$  point Brillouin zone, classified as  $A_1 + E_1 + 2E_2$  modes (Raman actives),  $2B_1$  modes (Raman silent) and  $A_1 + E_1$  modes (infrared active) with single crystalline ZnO

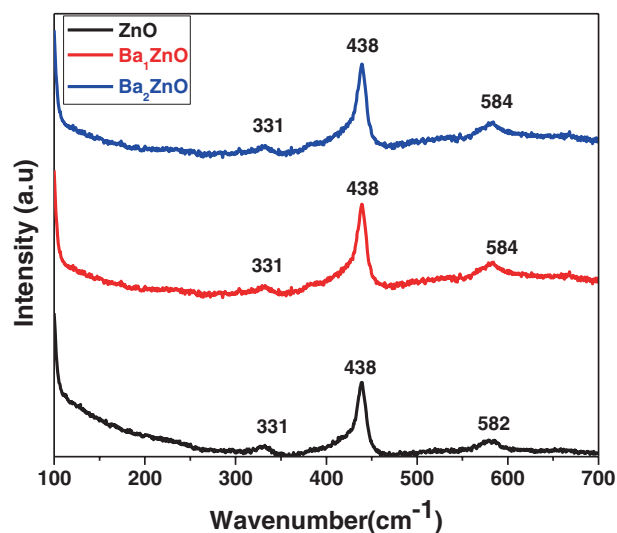


**Figure 7.** Raman spectra of Ba-doped and undoped ZnO nanoparticles.

corresponds to  $C_{6v}^4$  space group. The two polar modes denoted as  $E_1$  and  $A_1$  are split into longitudinal optical (LO) and transverse optical (TO) branches [35]. As we can see in figure 7, three main Raman peaks are observed. The modes at 331, 438 and 582  $\text{cm}^{-1}$  are assigned to  $E_{2H}-E_{2L}$ ,  $E_{2H}$ ,  $E_1(\text{LO})$  modes, respectively. The second-order vibration mode observed at 331  $\text{cm}^{-1}$  frequency arises from  $E_{2H}-E_{2L}$ . The strongest and sharpest peak was found to be around 437  $\text{cm}^{-1}$  and can be attributed to the high-frequency branch of the  $E_2$  (high) mode of ZnO, which represent the wurtzite crystal structure, the main Raman mode. It is associated with the sensitivity of internal stress and motion of oxygen atoms [36,37]. Origin of the above mode may be due to the Zn interstitial. The band observed at 573  $\text{cm}^{-1}$  belongs to the  $E_1$  (LO) modes. It is well known that  $E_1(\text{LO})$  peak is due to defects due to O-vacancies, Zn-interstitials or these complexes, and free carriers and is associated with the formation of defects in the nanoparticles [38,39]. Moreover, the Raman peak of  $E_1(\text{LO})$  obviously shifts towards a wavenumber from 582  $\text{cm}^{-1}$  of pure ZnO to 584  $\text{cm}^{-1}$  for Ba-doped ZnO. Its peak shifts towards higher wave number probably due to impurity effects, in accordance with the results of XRD analysis [40].

#### 4. Conclusion

Undoped and Ba-doped ZnO nanoparticles were obtained by sonochemical synthesis method. The XRD peaks corresponding to ZnO were in good agreement with the standard JCPDS data. The XRD results clearly

showed the incorporation of  $\text{Ba}^{2+}$  ions into the ZnO lattice. The calculated crystallite size depicted that all the samples are in nanometer scale. SEM analysis shows the variation of particles size in the range of 12–26 nm. EDX analysis demonstrated the presence of Ba, O and Zn in the sample. The FTIR and Raman spectroscopy studies of Ba-doped ZnO and undoped ZnO NPs exhibited the existence of the distinct characteristic absorption peak for Zn–O stretching modes. The room-temperature PL spectra exhibit a strong ultraviolet emission of 330 nm, and the weak blue and green emission peaks were observed at 417 and 560 nm respectively. The UV–Vis absorption spectrum of the sample obtained with 2 at% of Ba, showed the lowest absorbance in the visible region. UV–Vis transmittance analysis shows high transmittance of  $\text{Ba}_2\text{ZnO}$  sample which suggests that this sample has good transparency, especially above 400 nm wavelength. Also, the high optical transparency provides suitable potential in organic solar cells or future optoelectronic nanodevice applications.

#### Acknowledgement

The authors are grateful to the Centre for Science & Technology of the Non-Aligned and Other Developing Countries (NAM S&T Centre), Department of Science and Technology, India for financial support.

#### References

- [1] S J Pearton, D P Norton and F Ren, *Small* **3**, 1144 (2007)
- [2] X L Hu, Y J Zhu and S W Wang, *Mater. Chem. Phys.* **88**, 421 (2004)
- [3] J Yang, J Lang, L Yang, Y Zhang, D Wang, H Fan, H Liu, Y Wang and M Gao, *J. Alloys Compd.* **450**, 521 (2008)
- [4] Ken Elen, Heidi Van den Rul, An Hardy, Marlies K Van Bael, Jan D'Haen, RoosPeeters, Dirk Franco and Jules Mullens, *Nanotechnol.* **20**, 055608 (2009)
- [5] R Yousefi, M R Muhamad and A K Zak, *Curr. Appl. Phys.* **11**, 767 (2011)
- [6] P Jajarmi, *Mater. Lett.* **63**, 2646 (2009)
- [7] R Song, Y Liu and L He, *Solid State Sci.* **10**, 1563 (2008)
- [8] Z H Wang, D Y Geng, Z Han and Z D Zhang, *Mater. Lett.* **63**, 2533 (2009)
- [9] P Mishra, R S Yadav and A C Pandey, *Ultrason. Sonochem.* **17**, 560 (2010)
- [10] M Sivakumar, A Towata, K Yasui, T Tuziuti and Y Iida, *Chem. Lett.* **35**, 60 (2006)
- [11] P Banerjee, S Chakrabarti, S Maitra and B K Dutta, *Ultrason. Sonochem.* **19**, 85 (2012)
- [12] D Sahu, B S Acharya and A K Panda, *Ultrason. Sonochem.* **18**, 601 (2011)
- [13] A Khorsand Zak, W H A Majid, H Z Wang, Ramin Yousefi, A Moradi Golsheikh and Z F Ren, *Ultrason. Sonochem.* **20**, 395 (2013)

- [14] JunGeng, Guang-Hui Song and Jun-Jie Zhu, *J. Nano Mater.* **2012**, 1 (2012)
- [15] R S Yadav, P Mishra and A C Pandey, *Inorg. Mater.* **46**, 163 (2010)
- [16] J Luo, J K Liang, Q L Liu, F S Liu, Y Zhang, B J Sun and G H Rao, *J. Appl. Phys.* **97**, 086106 (2005)
- [17] Nurul Syahidah Sabri, A K Yahya and Talari Mahesh Kumar, *AIP Conf. Proc.* **1328**, 268 (2011)
- [18] O Lupan, L Chow, L Ono, B Roldan Cuenya, G Chai, S Park, A Schulte and H Heinrich, *J. Phys. Chem. C* **114**, 12401 (2010)
- [19] C X Mei, J Yong, G X Yong and Z X Wei, *Chin. Phys. B* **11**, 21 (2012)
- [20] M Mahanti and D Basak, *AIP Conf. Proc.* **1447**, 713 (2011)
- [21] K S Suslick, S B Choe, A A Cichowlas and M W Grinstaff, *Nature* **353**, 414 (1991)
- [22] Chat Pholnak, Chitnarong Sirisathitkul, Sumentha Suwanboon and David James Harding, *Mater. Res.* **17**, 405 (2014)
- [23] M Palumbo, S J Henley, T Lutz, V Stolojan and S R P Silva, *J. Appl. Phys.* **104**, 074906 (2008)
- [24] J Fan and R Freer, *J. Mater. Sci.* **32**, 415 (1997)
- [25] E Ando and M Miyazaki, *Thin Solid Films* **516**, 4574 (2008)
- [26] G Srinet, R Kumar and V Sajal, *Mater. Lett.* **126**, 274 (2014)
- [27] Ali Reza Rajabi, Saeid Jabbarzare, Mohammad Reza Mohammad Shafiee and Majid Ghashang, *Curr. Nanosci.* **10**, 312 (2014)
- [28] R Elilarassi and G Chandrasekaran, *Mater. Sci. Semicond. Process* **14**, 179 (2011)
- [29] X L Wu, G G Siu, C L Fu and H C Ong, *Appl. Phys. Lett.* **78**, 2285 (2001)
- [30] R S Yadav, M Priya and C P Avinash, *Ultrason. Sonochem.* **15**, 5 (2008)
- [31] A Wang, B Zhang, X Wang, N Yao, Z Gao, Y Ma, L Zhang and H Ma, *J. Phys. D: Appl. Phys.* **41**, 215308 (2008)
- [32] H Li, J Wang and H Liu, *Vacuum* **77**, 57 (2004)
- [33] R Saleh, N F Djaja and S P Prakoso, *J. Alloy. Compd.* **546**, 48 (2013)
- [34] B S Rema Devi, R Raveendran and A V Vaidyan, *Pramana – J. Phys.* **68**, 679 (2007)
- [35] R Yousefi, F Jamali-Sheini, A K Zak and M R Mahmudian, *Ceram. Inter.* **38**, 6295 (2012)
- [36] B Cao, W Cai, H Zeng and G Duan, *J. Appl. Phys.* **99**, 073516 (2006)
- [37] L Duan, G Rao, Y Wang, J Yu and T Wang, *J. Appl. Phys.* **104**, 013909 (2008)
- [38] X Wang, Q Li, Z Liu, J Zhang, Z Liu and R Wang, *Appl. Phys. Lett.* **84**, 4941 (2004)
- [39] J Iqbal, X Liu, H Zhu, C Pan, Y Zhang, D Yu and R Yu, *J. Appl. Phys.* **106**, 083515 (2009)
- [40] G Singh, A K Srivastava, K Senthil, J S Tawale, M Deepa and K Yong, *J. Nanoengineering Nanomanufacturing* **1**, 77 (2011)